ISSN 1067-8212, Russian Journal of Non-Ferrous Metals, 2018, Vol. 59, No. 2, pp. 207–222. © Allerton Press, Inc., 2018.

REFRACTORY, CERAMIC, AND COMPOSITE MATERIALS

# Microstructural Evolution, Powder Characteristics, Compaction Behavior and Sinterability of Al 6061–$B_4C$ Composites as a Function of Reinforcement Content and Milling Times[1]

**Rafi Ud Din[a], *, Qaisar Abbas Shafqat[b], Zahid Asghar[a], G. H. Zahid[a], Abdul Basit[a], A. H. Qureshi[a], Tanvir Manzoor[a], Muhammad Ali Nasir[c], Fahad Mehmood[c], and Kaleem Imdad Hussain[d]**

[a] *Materials Division, Pakistan Institute of Nuclear Science and Technology (PINSTECH), Nilore, Islamabad, Pakistan*

[b] *Department of Physics, International Islamic University, Islamabad, Pakistan*

[c] *Department of Mechanical Engineering, University of Engineering and Technology Taxila, Pakistan*

[d] *Department of Biosciences, COMSATS Institute of Information Technology, Islamabad, Pakistan*

**e-mail: rafiuddin@pinstech.org.pk; rafi_682@yahoo.com*

Received July 18, 2017; in final form, December 15, 2017

**Abstract**—Al $6061_{100-x}$–$x$ wt % $B_4C$ ($x$ = 0, 5, 10, 20, 30 and 40) composites, prepared by mechanical alloying and compacted at room temperature, have been used for the present investigation. The effects of $B_4C$ content and milling time on the powder morphology, powder particle size, and other powder characteristics such as the apparent density, tap density, flow rate, cohesiveness, and hausner ratio are systematically investigated. The steady state of milling process is determined by observing the correlation between apparent densities and milling time explained by the morphological evolution of the powder particles during the milling process. The Hausner ratio (HR), estimated to evaluate friction between the particles, decreases with an increase in milling duration and $B_4C$ content due to the changes in morphology and hardness of the powders. The compressibility behavior of post-compacts as a function of compaction pressure and the $B_4C$ content was analyzed by using several linear and non-linear powder compaction equations. The linear Panelli and Ambrozio Filho, and non-linear Van Der Zwan and Siskens equations give the highest regression coefficients. The results are explained in terms of the plastic deformation capacity and plastic deformation coefficient of the powders, which are influenced by the hardness and the morphology of the powder. After compaction, the supersolidus liquid phase sintering was performed at various temperatures (585, 610 and 630°C) under high purity nitrogen atmosphere. The results revealed that the sinterability was degraded by increasing the reinforcement content, particularly above 10 wt % $B_4C$. Neutron radiography measurements conducted on the rolled composite sheet have revealed the uniform distribution of $B_4C$ particles in the composite.

*Keywords:* composites, mechanical alloying, compaction behavior, compaction equations, sintering, hardness

**DOI:** 10.3103/S1067821218020098

## 1. INTRODUCTION

Aluminum metal matrix composites (Al MMCs) have been the subject of extensive research due to its light weight, high strength, low co-efficient of thermal expansion, and good wear resistance properties. Nevertheless, the low elastic modulus of aluminum alloys limits its use in many load-bearing applications. Metal matrix composites (MMCs) reinforced with ceramic phase have attracted greatest interests owing to the combined effects of metallic and ceramic materials. The unique combination of extremely high hardness, low specific gravity, and wear resistance makes boron carbide ($B_4C$) a candidate material for various applications. However, widespread use of $B_4C$ is restricted due to its low fracture toughness. $B_4C$ reinforced aluminum matrix composites offer several advantages due to their high specific-strength, stiffness, wear resistance and low thermal expansion coefficient. Al–$B_4C$ composites are widely used as structural neutron absorber, armor plate materials, and as a substrate material for computer hard disks [1–4]. During recent years, due to the high neutron absorption cross-section of $^{10}B$ isotope, Al–$B_4C$ composite has been extensively used as excellent neutron absorber material to fabricate inside baskets of storage and transport containers of the spent nuclear fuel [5, 6].

Al MMCs can be generally prepared by liquid state processing, semisolid processing, and powder metallurgy (P/M) [7–20]. Among all the processes, powder metallurgy method is greatly reported to avoid detri-

[1] The article is published in the original.

mental interfacial reaction between matrix and reinforcement and also renders the possibilities of using reinforcement in higher amounts [9, 11–19]. During P/M process, the mixing process of matrix and reinforcement is an important step to acquire the homogeneous distribution throughout the consolidated composite materials. In this regard, mechanical alloying (MA) technique improves the particle distribution by incorporating the reinforcement particles into metal matrix in close distance [20–22]. Naiqin et al. have shown that MA renders homogeneous distribution of SiC reinforcement in the Al 6061 matrix [21]. M. Khakbiz et al. have investigated the simultaneous effects of $B_4C$ contents and milling times on the resultant grain size of Al–$B_4C$ composites [11]. Alizedah et al. have explored the role of nanosize reinforcements on mechanical milling stages in Al–4 wt % $B_4C$ nanocomposites [23]. In another investigation, it is found that milling time as well as reinforcement size strongly affects the particle size and microhardness of Al2024–$B_4C$ composite powders [16]. Despite of available literature on the mechanical alloying of Al–$B_4C$ composites, there is the lack of the detailed investigations providing the understanding of the correlation among the milling parameters, the powder characteristics and the consolidation process.

The compressibility of composite powders is generally found to deteriorate with increase in reinforcement which ultimately deteriorates mechanical strength of bulk composites. Therefore, it is imperative to study and improve compressibility of composite powders in order to achieve higher density during compaction. So far, many studies for various composites [13, 14, 18, 20, 24, 25] and only one partial study for Al–$B_4C$ composites [23] have been carried out to investigate compressibility of composite powders containing micrometric reinforcement particles. Moreover, optimization of P/M processing route of Al–$B_4C$ composites requires detailed knowledge of flow parameters of powder particles such as apparent density, tap density, and true density affecting their compressibility. Nevertheless, detailed studies investigating flow characteristics as well as the compressibility of Al–$B_4C$ composite powders are still lacking in the literature.

During recent years, the use and derivation of empirical compaction equations have played an important role for evaluation of compaction behavior because density-pressure relationship of powder significantly affects microstructure of sintered compacts. Recently, compaction behavior of Al 6061–$TiO_2$ composites as a function of compaction pressure and nano titania content is investigated by using several linear and non-linear powder compaction equations [14, 18]. Moazami et al. have concluded that plastic deformation capacity of powders can be predicted reasonably by using Heckel and Panelli-Ambrozio equations [24]. The compressibility curves of AA 6061–TiC composite powders are investigated by using the Heckel, Panelli and Ambrosio and Ge equations. Alizedah et al. have studied compressibility of milled powder of Al–4 wt % $B_4C$ composite by using modified Heckel equation to consider the pressure effect on yield strength [23]. To the best of our knowledge, there is no other report investigating the compressibility of Al alloy/$B_4C$ reinforced composites by using compaction equations.

The main objective of present work is to investigate the effects of $B_4C$ contents and milling conditions on powder flow characteristics, powder surface morphology, compressibility, sinterability, and mechanical properties of Al 6061–$x$ wt % $B_4C$ ($x$ = 5, 10, 20, 30 and 40) composites prepared by MA and compaction followed by conventional consolidation technique. The correlation between relative density of compacts and uniaxial compaction pressure is evaluated experimentally and compared with those predicted by different numerical linear and non-linear compaction models.

## 2. EXPERIMENTAL

Fine, gas atomized 6061-Al alloy powder with mean particle size 19 μm and boron carbide powder with mean particle size of 8 μm were used as starting materials. Results of laser particle size analysis for boron carbide powder have been given in supplementary information Fig. S1. Table S1 gives the composition of 6061-Al alloy.

The composite powders of AA $6061_{100-x}$–$x$ wt % $B_4C$ ($x$ = 0, 5, 10, 20, 30 and 40) were produced by MA. MA was carried out in a planetary ball mill PM 4, developed by RETSCH (Germany) up to 15 h to ensure the process has reached its steady state. During milling a charge ratio (weight of the powder to the weight of the balls) of 1 : 10 was used. Stearic acid (0.02 wt %) was added as process control agent (PCA) and milling was performed at 200 rpm under argon atmosphere to avoid oxidation of newly exposed surface. The ball milled powders were characterized by their morphology (i.e. shape), apparent density, tap density, and flow rate. The morphology of the milled powder particles was investigated by using the scanning electron microscope (SEM) of LEO 440 make. Figures S2a and S2b shows the morphologies of the as received Al matrix powder and $B_4C$ particles. The apparent density or random loose packing of a powder is determined by standard (ISO 3923) cup and funnel method, and the tap density or random dense packing of powder is measured by ETD-1020 Tap Density Tester. Standard Hall Flow meter was used to measure the flow rate of the powders. Averages of five independent measurements were carried for each density. The

experimental error in measuring densities was less than 5%. The particle size of composite powders was measured using laser scattering technique (Cilas 1064 laser particle size analyzer).

The milled composite powders were uniaxially pressed into disk type compacts of 19 mm diameter and larger size rectangular compacts (60 × 40 mm) under various compaction pressures with zinc stearate as the die lubricant. The samples were used to determine the compressibility curves of the powder after various milling times. Sintering was performed in two stages. In the first stage, the green compacts were heated in a tubular furnace under vacuum of $1 \times 10^{-1}$ mbar up to 400°C for 1 h to remove volatile species produced during burning of PCA. In the second stage, sintering was performed at various temperatures under $N_2$ atmosphere using a flow rate of 5 L/min and a dew point temperature of less than –42°C. After 1 h holding time, the furnace was cooled to room temperature in $N_2$ atmosphere. The density of sintered compacts was measured by Archimedes principle. The sintered 6061Al/$B_4C$ composite compacts were homogenized at 525°C for 1 h. After homogenization, compacts were hot rolled with thickness reduction of 5 to 15% per pass. Between the rolling passes compacts were heated for 20 min to reach 525°C and equilibrate. At the end of the rolling compacts received a total thickness reduction of more than 80%. Figure S3 shows the micrographs of sintered and rolled composites.

The sintered compacts after rolling were sectioned from the longitudinal cross section for metallographic studies. The polished surface of 6061Al/$B_4C$ was examined under Olympus BX51 optical microscope. Macroscopic hardness of sintered 6061Al/$B_4C$ composites was measured on Rockwell B (HRB) testing machine, using an initial load of 10 Kgf and major load of 90 Kgf with 1/16" steel ball indenter. The given values of hardness were average of five measurements on each sample.

Neutron radioscopy or radiography (NR) is a convenient method for determining the qualitative $B_{10}$ distribution of neutron absorber material (ASTM E94, E142, and E545). The present NR facility is installed at the radial beam-line 06 of the pool type PARR-1 Nuclear Research Reactor (PINSTECH, Islamabad, Pakistan) that operates at a power of 10 MW producing a thermal neutron flux of about $10^{13}$ n/s cm$^2$ near the reactor core. The main characteristics of the neutron beam at the irradiation position are listed in Table S2. Any inhomogeneity in the object or internal defects e.g. voids, cracks, porosity or inclusion will show up as a change in gray value/radiation intensity reaching the detector. The optical density readings, derived from the neutron radioscopy or radiography are measured with an optical densitometer (Model 07-424, S-23285).

## 3. RESULTS AND DISCUSSION

### *3.1. Morphological and Particle/Agglomerate Size Analysis of Composite Powders*

The compressibility behavior of powders and consolidation process of P/M products is greatly influenced by powder characteristics such as morphology, microstructure, apparent density, flowability, hardness, particle size, and particle size distribution. Figures 1a–1f exhibits the morphology of Al 6061–10 wt % $B_4C$ composite powder as a function of milling time (1, 4, 8, 12 and 15 h). After 4 and 8 h of milling (Figs. 2, 1b, 1c), several flattened and welded particles are formed. During this stage of milling, the predominant mechanism (up to 8 h) is plastic deformation that leads to a change in particle shape and cold welding which increases the particle size. Further milling results in with the morphological transformation from flattened to near-equiaxed particle morphology. As the ball milling is further prolonged, the fracturing predominates over other processes owing to decrease in the plastic deformation capability of particles. The fracturing process leads to the reduction of matrix particle size until equilibrium is reached between cold welding and fracturing [26]. After 12 h of milling (Fig. 1d), the particle size decreases sharply with the equiaxed and spherical morphology. The formation of almost equiaxed particles indicates that the milling has approached to the steady-state condition. Further, Fig. 1f displays the magnified image of powder morphology following 15 h of milling. It is vividly discernible that the boundary division between $B_4C$ particles and the soft Al alloy is inconspicuous. It is envisaged that the $B_4C$ particles act as a milling agent in addition to the other milling media. Two important mechanical properties of $B_4C$, which are relevant here, are its high hardness and the strength as typified by the Young's modulus of ~0.47 TPa. Due to the rigorous ball milling, the $B_4C$ particles will undergo repeated collisions with Al alloy matrix. Because of the high hardness and strength, the carbide particles may penetrate in alloy matrix.

The effect of reinforcement addition on the matrix morphology and agglomerate size of composite powder after 12 h of milling is shown in Figs. 2a–2e. The results indicate that the agglomerate size of the composite powders decreases considerably as a function of the $B_4C$ contents added. However, almost spherically shaped and equiaxed particles are observed in all systems with the same milling time of 12 h. It is concluded that for longer milling time such as 12 h (Fig. 1), the fracturing process predominates cold welding of particles favoring refining of matrix particles. Moreover, it is afore-mentioned that high hardness and strength of $B_4C$ may penetrate them into alloy matrix resulting in their work hardening and enhancing fracturing mechanism. These results are further corroborated by the particle size analysis pre-

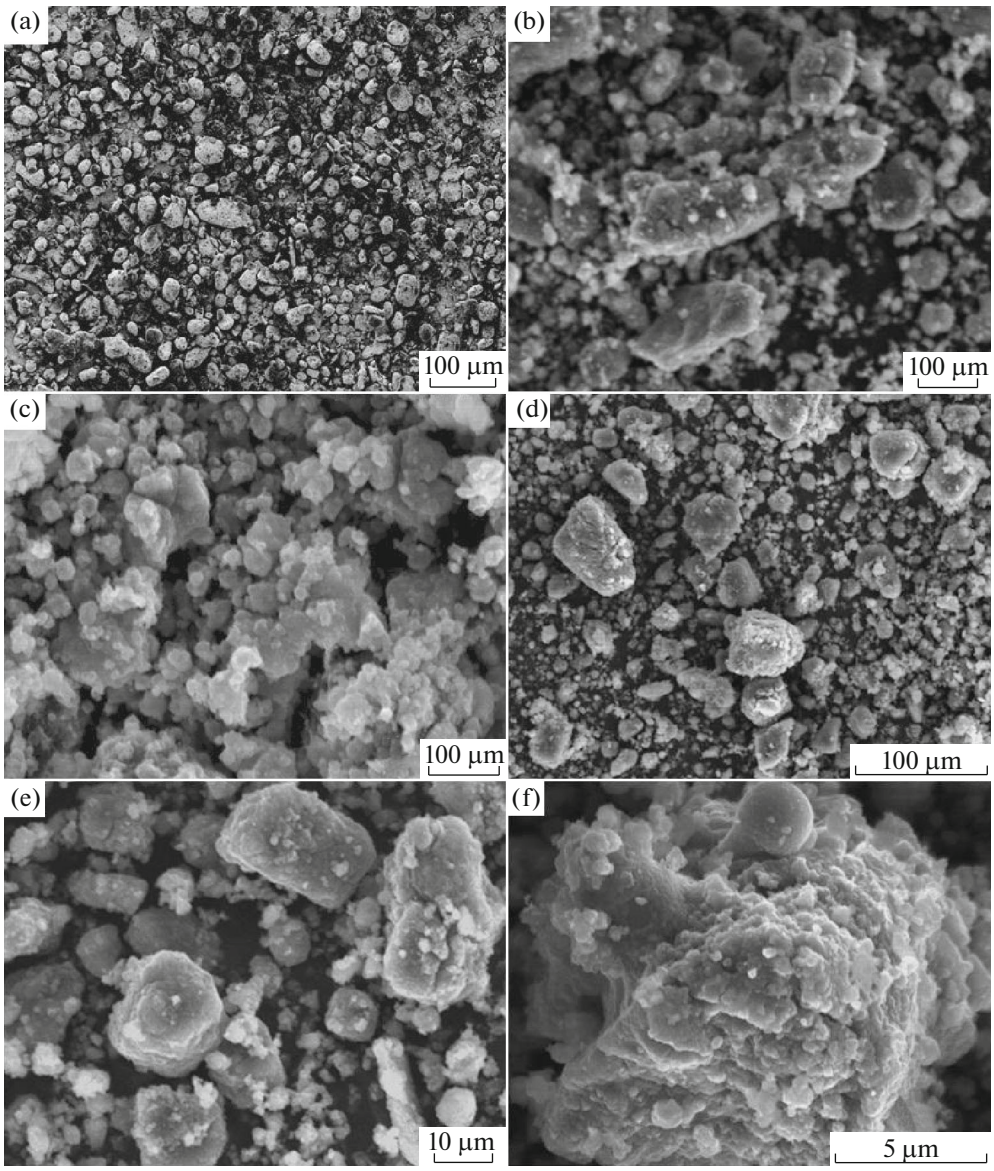


**Fig. 1.** Morphology of Al 6061–10 wt % $B_4C$ composite powder after (a) 1 h, (b) 4 h, (c) 8 h, (d) 12 h, (e) 15 h milling, and (f) magnified image after 15 h milling.

sented in Table 1. The mass median diameter ($D_{50}$) of produced powders decreases with increase in addition of $B_4C$ particles. Particle size distribution of powders can be precisely characterized by geometric standard deviation ($\sigma_g$) of log normal distribution given by following equation [27]:

$$\sigma_g = D_{84.1}/D_{50}. \quad (1)$$

Where $D_{50}$ is mass median particle diameter and $D_{84.1}$ is diameter of particle that is equal or less than 84.1% of the mass of present particles on the cumulative mass distribution plot. The calculated values of $\sigma_g$ are shown in Table 1. The particle size distribution of particles becomes broader with increase in reinforcement. As hard $B_4C$ particles easily penetrate into soft alloy matrix resulting in decreased volume fraction of free $B_4C$ particles within powder mixture leading to an increased overall particle size distribution.

**Table 1.** Average particle size and particle size distribution of Al 6061–$x$ wt % $B_4C$ ($x$ = 0, 5, 10, 20, 30, 40) composite powders

| Powder | $D_{50}$, μm | $\sigma_g$ |
|---|---|---|
| 6061Al Alloy | 18.7 | 38.4 |
| 6061AA + 05% $B_4C$ | 33.1 | 2.61 |
| 6061AA + 10% $B_4C$ | 27.6 | 2.65 |
| 6061AA + 20% $B_4C$ | 20.3 | 2.86 |
| 6061AA + 30% $B_4C$ | 14.9 | 3.52 |
| 6061AA + 40% $B_4C$ | 10.1 | 3.60 |

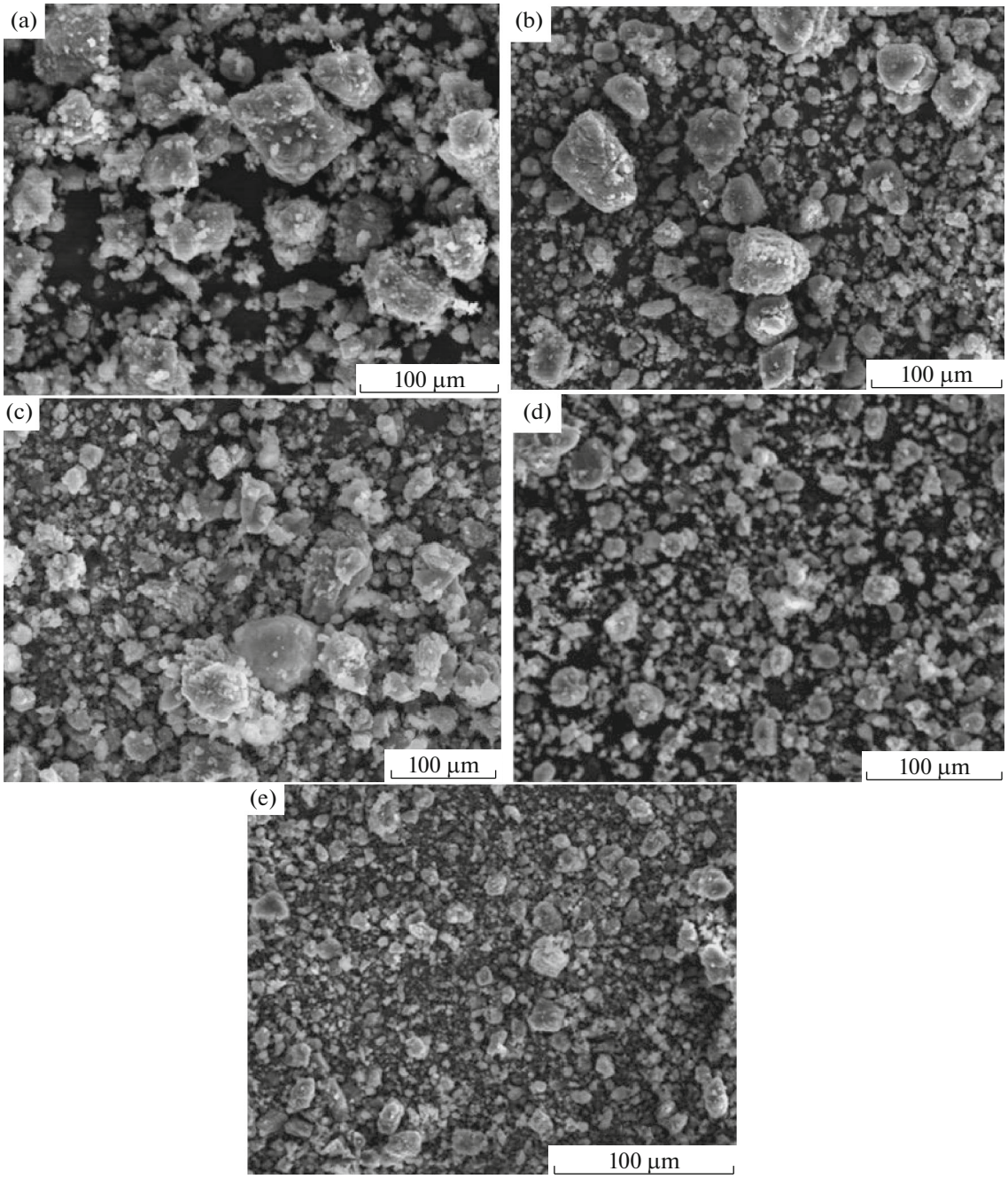


**Fig. 2.** Morphology of (a) Al 6061–5 wt % $B_4C$, (b) Al 6061–10 wt % $B_4C$, (c) Al 6061–20 wt % $B_4C$, (d) Al 6061–30 wt % $B_4C$, and (e) Al 6061–40 wt % $B_4C$ composite powders after 12 h milling.

### *3.2. Powder Characteristics (Apparent Density, Tap Density, Hausner Ratio, Cohesiveness, and Flow Rate)*

The evolution of apparent density, Hausner ratio, and flow rate of composite powders with milling time is presented in Fig. 3. The apparent density at zero hours of milling implies the apparent density of as-received powder in case of unreinforced metal alloy, and manually mixed powders in case of composite powders. It is obvious in Fig. 3a that as-received powder has a higher apparent density than manually mixed composite powders. There is a continuous decrease in apparent density of unreinforced AA 6061 with increasing milling time. The apparent density reaches a minimum value at 8 h of milling time, and then starts to increase with further increase in milling time and it reaches a steady value near to that of the as-received powder after longer milling times. The incorporation of $B_4C$ renders a similar behavior of apparent density

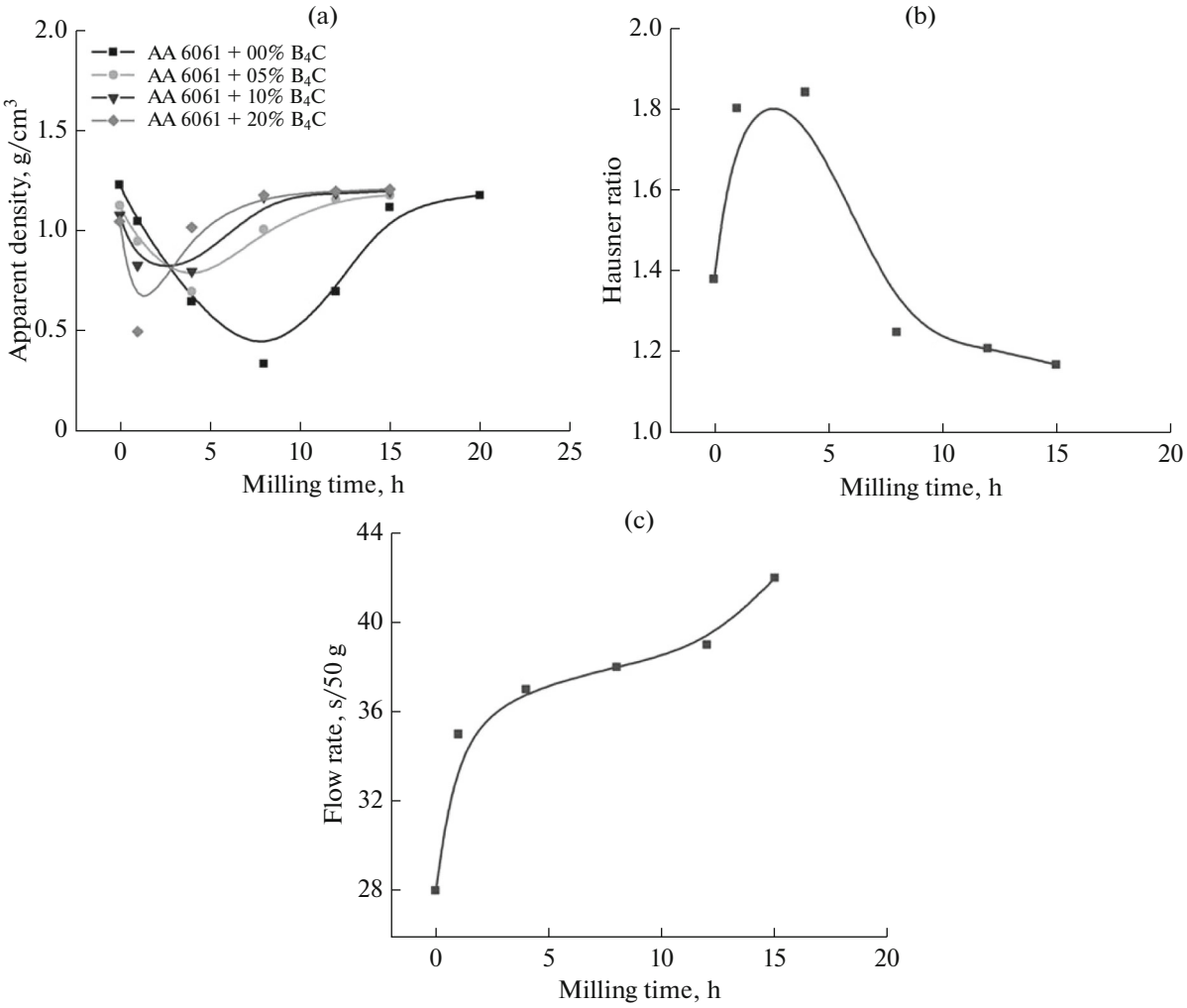


**Fig. 3.** (a) Apparent density of Al 6061–*x* wt % $B_4C$ ($x = 0, 5, 10, 20$) composite powders, (b) Hausner ratio, and (c) Flow rate of Al 6061–10 wt % $B_4C$ composite powder as a function of milling time.

curve albeit this behavior completes in a much shorter time compared to that of unreinforced Al 6061. The presence of reinforcement particles accelerates the evolution of the apparent density with milling time. It is evident that the addition of 10% $B_4C$ brings this in about half the time it takes with the unreinforced Al 6061 powder alloy. This effect is further enhanced with 20% $B_4C$. This behavior of apparent density with milling time is obviously associated with the morphological changes of powder particles during milling (see Fig. S2). The equiaxial or quasi-spherical morphology of as received alloy powder (see Fig. 1) and the long-time-milled powders (see Fig. 1) allows good powder packing resulting in their high apparent density. On the other hand, the flattened morphology and cold welding of the short-time-milled powders (see Fig. 1) explains for their low apparent density. Hausner ratio, which is a useful measure of cohesion, is defined as the ratio between the tap density and the apparent density of powders. It is evident in Fig. 3b that the Hausner ratio increases upto 4 h of milling and then drastically decreases. It has been already indicated that upto 4 h of milling yields flattened particles with less specific surfaces, which explains the increase in Hausner ratio upto 4 h of milling. The cohesivity in terms of Hausner ratio with milling times above 4h decreases drastically due to work hardening effect of the powder caused by the more specific surfaces of composites powders. The flow rate of composite powder increases with milling time owing to changes in the powder morphology (Fig. 3c). A sharp increase has been observed upto 4 h of milling, which may be attributed to evolution of irregular flattened morphology resulting in increased friction among particles. Above 4 h milling, steady increment in flow rate arises from different size distributions caused by the refinement of particles.

The effects of $B_4C$ contents added on the apparent density, the tap density, Hausner ratio, cohesiveness, and flow rate of Al 6061/$B_4C$ powders are shown in Fig. 4. The apparent density decreases with an

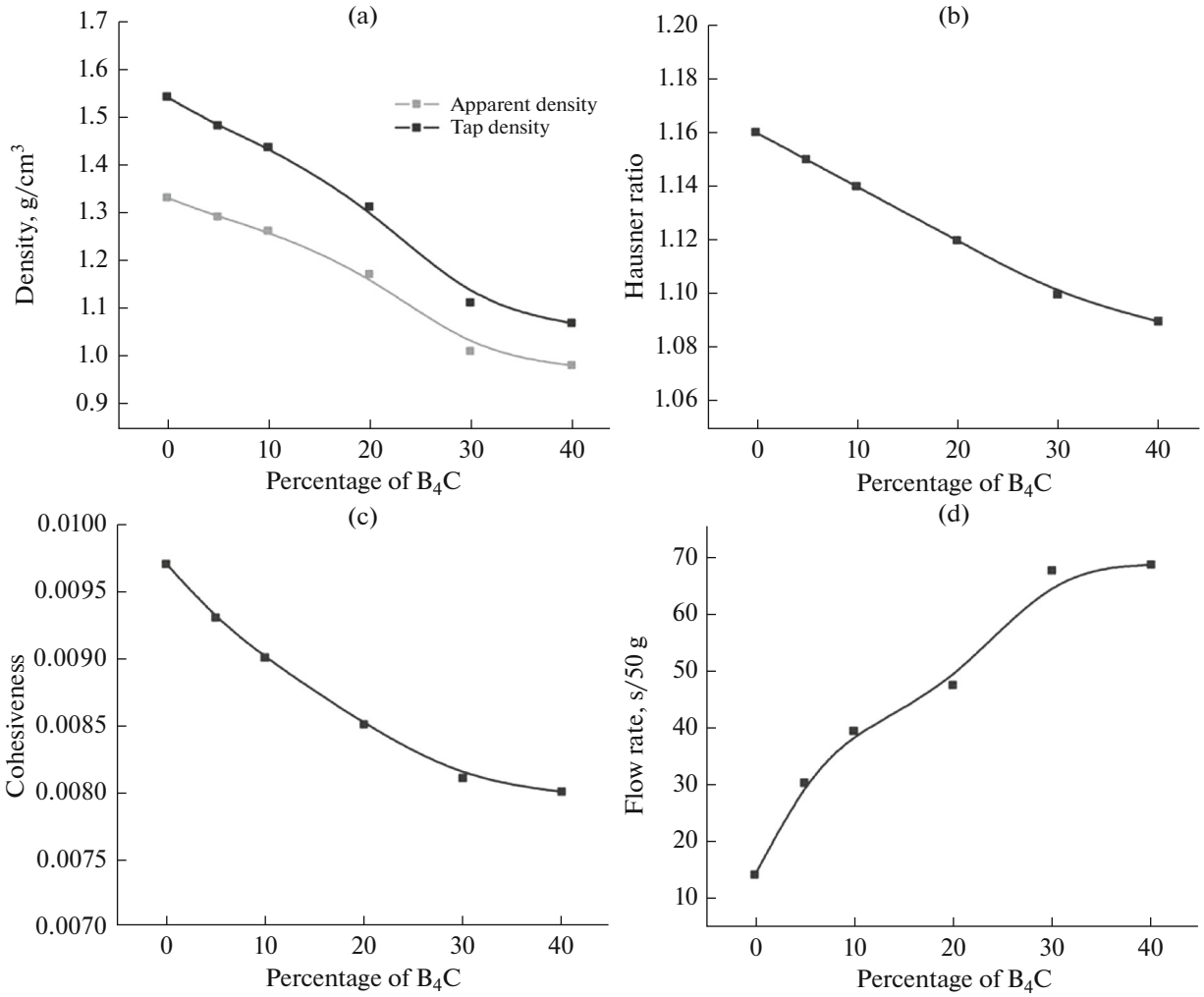


**Fig. 4.** Characteristics of Al 6061–$x$ wt % $B_4C$ ($x$ = 0, 5, 10, 20, 30, 40) composite powders (a) apparent density and tap density (b) hausner ratio, (c) cohesiveness, and (d) flow rate.

increase in $B_4C$ contents. As it is already mentioned that apparent density of milled powders is closely related to their morphology and particle size distribution. The flattened and irregular morphology of powders with large particle size distribution renders a poor packing due to increase in the internal friction between the particles. On the contrary, the equiaxial and almost spherical shaped milled powders provide good packing. An increase in $B_4C$ contents increases the internal friction between the particles due to large particle size distributions (Table 1) that results in decrease in apparent density and vice versa. Tap density has also exhibited similar behavior to that of apparent density. It also decreases with an increase in $B_4C$ contents, which is ascribed to powder morphology changes and more work hardening caused by the more specific surfaces of milled powders. It is obvious in Fig. 4b that the Hausner ratio decreases as $B_4C$ contents increases. It implies that incorporation of ceramic phase significantly reduces the cohesivity. This phenomenon is again attributed to the work hardening of powders i.e. more specific surface of the milled powders. The cohesiveness of the Al 6061/$B_4C$ composite powders is also analyzed by using Kawakita equation [28]. The Kawakita equation is used to study powder compression using the degree of volume reduction ($C$):

$$C = (V_0 - V)/V = abP/1 + bP. \quad (2)$$

The equation, in practice, can be arranged as:

$$P/C = P/a + 1/ab. \quad (3)$$

Where a and b are constants; $1/b$ is considered to be a constant related to cohesion and is called cohesiveness. Numerical values for constants $a$ and $b$ are obtained from the slope ($1/a$) and the intercept ($1/ab$) of plots of $P/C$ against number of taps $P$. The cohesiveness obtained by Kawakita equation as the function of reinforcement is also presented in Fig. 4c which displays the same phenomena as depicted by Fig. 4b.

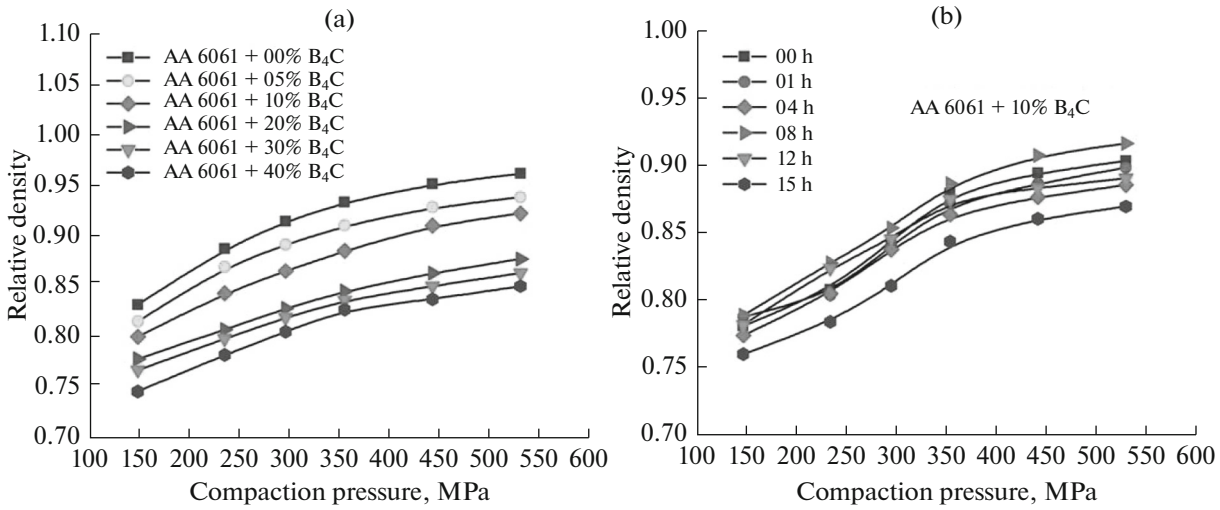


**Fig. 5.** Compressibility curves of (a) Al 6061–$x$ wt % $B_4C$ ($x = 0, 5, 10, 20, 30, 40$) composite powders and (b) Al 6061–10 wt % $B_4C$ composite powder at different milling times.

Figure 4d indicates that the flow rate of milled powders increases with an increase in the percentage of $B_4C$. This poor fluidity of composite powders, rendered by the introduction of $B_4C$ particles, is attributed to the increased friction among particles arising from irregular powder morphology or larger particle size distributions as stated earlier.

### *3.3. Investigation of Densification and Compressibility Behavior of Composite Powders*

The characteristics of composite powder strongly influence the compaction behaviour. In order to optimize the consolidation process as well as the composition of the mixture, it is imperative to anticipate the densification behavior of composites under pressure. It is generally believed that spherical and equiaxed particles yield symmetrical opposite forces at the contact points of particles promoting compressive deformation of particles. Therefore, such powders are considered very hard to compact owing to high internal friction between particles. On the contrary, irregular-shaped particles yield the asymmetric opposite forces at the contact points between particles resulting in the shear deformation that leads to decrease of compaction pressure for densification [18, 26]. The compressibility curves of Al 6061–$x$ wt % $B_4C$ ($x = 0, 5, 10, 20, 30$ and 40) composite powders, compacted at different pressures, are shown in Fig. 5a. With an increase in the compaction pressure, the density increases with a decelerating rate. Moreover, it is evident that the green density decreases with an increase in the percentage of reinforcement. The decelerating rate as function of composition is constant upto 10 wt % $B_4C$ additions. A sharp increase in decelerating rate is observed for reinforcement contents of more than 10 wt %. The relative density decreases with the percentage of reinforcement due to work hardening effect and morphology changes during mechanical milling. The unreinforced Al 6061 alloy powder exhibits the highest compressibility due to its irregular morphology (larger particle size distribution). Based on the experimental results, the response of powders under uniaxial pressing can be divided into two stages. The densification increases abruptly during the first stage. Then, in the second stage the densification increases steadily. The particle rearrangement by interparticle sliding is known as the mechanism of first stage whereas the second stage initiates as the particle interlocking renders the plastic deformation. The results indicate that first stage completes below 350 MPa compaction pressure due to equiaxed and almost spherical shaped powder beyond which the densification is achieved only because of plastic deformation. The incorporation of $B_4C$ considerably reduces matrix particle size that results in lowering of relative density at low compaction pressures due to work hardening effect. At high compaction pressure, rate of decreased relative density in the plastic deformation domain is higher than the particle rearrangement domain due to drastic powder morphology reduction. Moreover, an increase in $B_4C$ contents decreases the plastic deformation capacity of the matrix at plastic deformation stage due to stress shielding effect of $B_4C$ contents.

The results presented so far indicate that addition of $B_4C$ influences consolidation behavior of Al alloy powder. These effects significantly depend on powder characteristics and method of powder preparation, i.e. mechanical milling. The typical compressibility behavior of AA 6061–10 wt % $B_4C$ as a function of milling time is shown in Fig. 5b. It is obvious that 8 h milled composite powders provide the higher densification compared to that of manually mixed as well as other milled composite powders. The density of the manually mixed powder is higher than that of the 1, 4, 12, and 15 h milled composite powders. It is envisaged

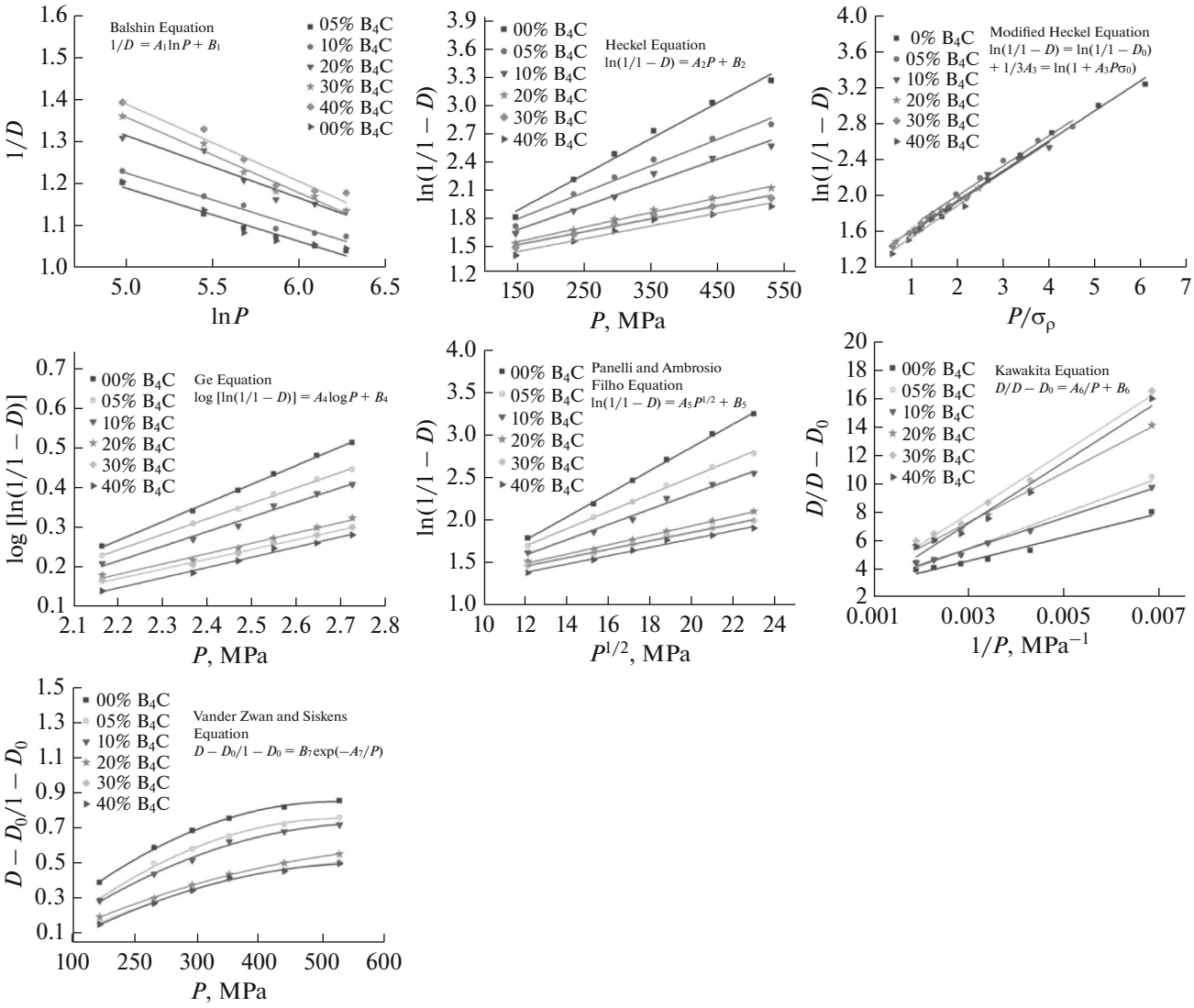


**Fig. 6.** Experimental compressibility data of Al 6061–$x$ wt % $B_4C$ ($x$ = 0, 5, 10, 20, 30, 40) composite powders fitted by various linear and non-linear compaction equations.

that clusters and agglomerates of $B_4C$ particles in manually mixed powders are disintegrated under applied load and fill voids between bigger particles. Since $B_4C$ particles have penetrated alloy matrix (Fig. 2) for longer times milled powders, therefore, theses particles cannot contribute in rearrangement process. It is expected that irregular powder morphology of 8 h milled powders arising from its flattening and cold welding provides a higher densification of these powders as compared to the other milled powders.

### *3.4. Quantitative Evaluation of Compaction Equations for Compressibility Data of Composites*

The quantitative evaluation of compaction behaviour in terms of plastic deformation capacity during the consolidation process is generally carried out by employing linear and non linear compaction equations. A compaction equation relates various consolidation parameters, such as the porosity and relative density to the compaction pressure [14]. To evaluate role of $B_4C$ contents on consolidation of AA 6061/$B_4C$ powders, various empirical compaction equations, proposed by various authors [13, 14, 18], are employed and fitting results of experimental compressibility data to these equations are shown in Fig. 6. Balshan equation is one of the simplest equations given by:

$$1/D = A_1 \ln P + B_1. \quad (4)$$

Heckel has provided the most commonly used model for prediction of densification behavior of metal powders:

$$\ln(1/1 - D) = A_2P + B_2. \quad (5)$$

**Table 2.** Comparison of various parameters derived from linear and non-linear compaction equations of Al 6061–$x$ wt % $B_4C$ ($x$ = 0, 5, 10, 20, 30, 40) composite powders after 8 h milling

| Model | Type | AA 6061 + 0% $B_4C$ | AA 6061 + 05% $B_4C$ | AA 6061 + 10% $B_4C$ | AA 6061 + 20% $B_4C$ | AA 6061 + 30% $B_4C$ | AA 6061 + 40% $B_4C$ |
|---|---|---|---|---|---|---|---|
| Bashan | $A_1$ | 0.1281 | –0.1286 | –0.1451 | – 0.1489 | –1.1806 | 1.1850 |
| | $R^2$ | 0.9235 | 0.9518 | 0.9809 | 0.9156 | 0.9687 | 0.9283 |
| Heckel | $A_2(10^{-3})(\sigma_0)$ | 3.86 (86.35) | 2.86 (116.55) | 2.54 (131.23) | 1.57 (212.31) | 1.40 (238.10) | 1.38 (241.54) |
| | $D_0$ | 0.7382 | 0.7229 | 0.7192 | 0.7105 | 0.7015 | 0.6965 |
| | $R^2$ | 0.9858 | 0.9764 | 0.9737 | 0.9936 | 0.9790 | 0.9534 |
| Modified | $\sigma_0$(MPa) | 76.27 | 95.84 | 109.20 | 158.73 | 175.44 | 182.49 |
| Heckel | ν | 0.3170 | 0.3203 | 0.3265 | 0.3318 | 0.3330 | 0.3401 |
| | $R^2$ | 0.9060 | 0.9761 | 0.9735 | 0.9926 | 0.9795 | 0.9501 |
| Ge | $A_4$ | 0.4753 | 0.3938 | 0.3722 | 0.2633 | 0.2473 | 0.2595 |
| | $R^2$ | 0.9985 | 0.9928 | 0.9842 | 0.9820 | 0.9826 | 0.9850 |
| Panelli | $A_5$ | 0.1372 | 0.1018 | 0.0901 | 0.0556 | 0.0449 | 0.0494 |
| | $R^2$ | 0.9986 | 0.9971 | 0.9856 | 0.9956 | 0.9949 | 0.9818 |
| Kawakita | $A_6$ | 83.93 | 124.83 | 110.60 | 176.04 | 218.11 | 216.67 |
| | $R^2$ | 0.9644 | 0.9794 | 0.9900 | 0.9964 | 0.9885 | 0.9721 |
| Van der | $A_7$ | 0.2293 | 0.3489 | 0.6595 | 0.8016 | 0.8718 | 0.9248 |
| Zwan | $B_7$ | 335 | 305 | 274 | 179 | 194 | 219 |
| | $R^2$ | 0.9972 | 0.9973 | 0.9919 | 0.9987 | 0.9976 | 0.9916 |

Where $D$ is relative density of compact, $P$ is applied pressure, and $A_2$ and $B_2$ are constants. Heckel has shown an empirical relation between $A_2$ and yield strength ($\sigma_0$) of material as follows:

$$A_2 = 1/3\sigma_0. \quad (6)$$

The term $3\sigma_0$ is known as yield pressure. $A_2$ can be substituted by $\ln(1/(1 - D_0))$, where $D_0$ is relative density at $P = 0$. Denny has modified Heckel equation by considering the pressure dependency of yield stress in the equation. As a result, $\sigma_0$ could be obtained via the following linear equation:

$$\sigma = \sigma_0 + AP. \quad (7)$$

Where $\sigma$ is yield stress at pressure $P$. The modified Heckel equation can be written as:

$$\ln(1/1 - D) = \ln(1/1 - D_0) + 1/3A_3\ln(1 + A_3P/\sigma_0). \quad (8)$$

By assuming that the compact is isotropic and perfectly elastic, Denny has proposed an equation relating term $A_3$ to Poison's ratio (ν):

$$A_3 = 2\nu^2/1 - \nu. \quad (9)$$

Ge has proposed another compaction equation

$$\log[\ln(1/1 - D)] = A_4\log P + B_4. \quad (10)$$

Another useful compaction equation is proposed by Panelli and Ambrozio Filho:

$$\ln(1/1 - D) = A_5P^{1/2} + B_5. \quad (11)$$

Where $A_5$ and $B_5$ are constant and related to characteristics of powder. Parameter $A_5$ is used for the evaluation of powder plastic deformation capacity, and $B_5$ can be used for the determination of relative density at $P = 0$. Another linear compaction equation that considers relative apparent density ($D_0$) is suggested by Kawkita:

$$D/D - D_0 = A_6/P + B_6. \quad (12)$$

The linear compaction equations (4), (5), (8), (10), (11), and (12) were fitted to the compaction data using "least squares-linear" method (Fig. 6). A non-linear equation, proposed by Van Der Zwan and Siskens obtained from Cooper and Eaten, is also applied to our compaction data:

$$D - D_0/1 - D_0 = B_7\exp(-A_7/P). \quad (13)$$

The constant $A_7$ represents rate of plastic deformation coefficient whereas constant $B_7$ represents magnitude of pressure at start of plastic deformation.

The compaction equations, presented here, are used to evaluate the compaction behavior of fabricated composites in terms of particle rearrangement by particle sliding and plastic deformation by particle interlocking quantitatively. Both linear and non-linear compaction equations are tested with and without considering $D_0$ (depends upon equations) in this work. Based on the analysis of compaction equations (both linear and non-linear), Table 2 indicates that the linear Panelli and Ambrozio Filho Eq. (11) and non-linear Van Der Zwan and Siskens Eq. (13) give the highest regression coefficients $R^2$ (0.9927 and 0.9975). The results of statistical quantitative analysis, performed on experimental data of the developed composite

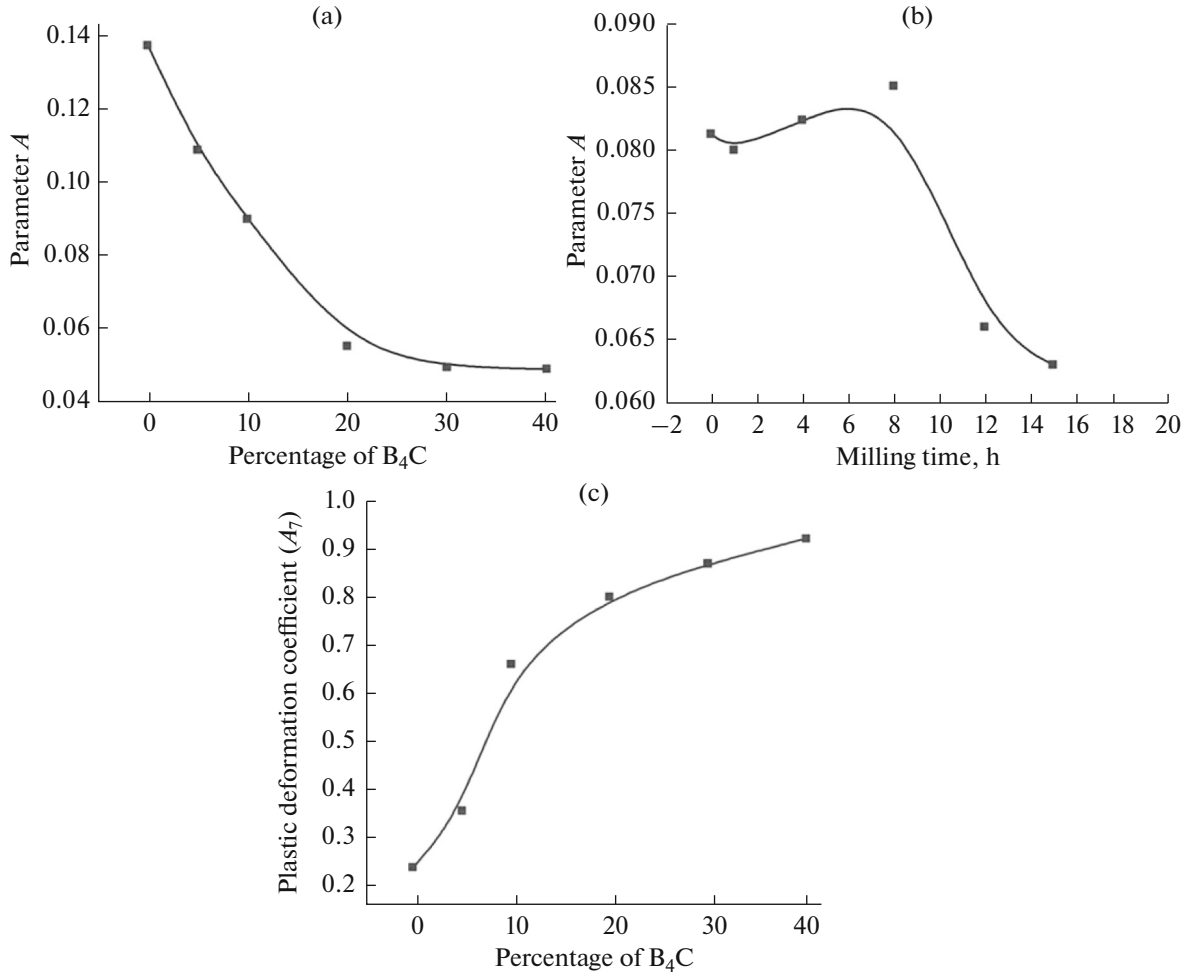


**Fig. 7.** (a) Parameter *A* as a function of $B_4C$ added, (b) Parameter *A* of Al 6061–10 wt % $B_4C$ as a function of milling time, and (c) Plastic deformation coefficient as a function of $B_4C$ added.

powders, are summarized in Table 2. The calculated ν and $\sigma_0$ values via the heckel and modified heckel equations are also shown in Table 2. An increase in $B_4C$ contents increases the yield stress ($\sigma_0$) value. Parameter *A*, inclination or slope from the linear plot, provides the plastic deformation capacity of the powder in compaction. Figure 7a indicates that addition of hard nanoparticles decreases plastic deformation capacity due to load partitioning effect. The presence of hard reinforcement particles restricted the deformation capacity of alloy matrix leading to decrease of parameter *A*. Figure 7b depicts the parameter *A* from Eq. (11) as a function of milling time of Al 6061 with 10 wt % $B_4C$. The reinforced powders without milling exhibit highest values of plastic deformation capacity. The material, consisting of soft aluminium alloy and hard ceramic particles, is deformed as a whole during pressing and the ceramic particles do not undergo significant deformation. During pressing, alloy morphology deviates from equiaxed shape due to local deformation rendered by hard ceramic particles and, consequently, ameliorates the compressibility. The increase of parameter A after short milling times indicates that flattened and cold-welded morphology provides a higher deformation capacity during pressing. With short milling times, the effect of morphology preponderates, and parameter A decreases after 8 h milling due to morphology changes and work hardening due to long milling times. The effects of reinforcement additions on rate of powder plastic deformation coefficient, derived from Van Der Zwan and Siskens Eq. (13), is shown in Fig. 7c. It is obvious in Fig. 7c that rate of plastic deformation coefficient increases with $B_4C$ additions. It is ascribed to morphology changes and refined particle size rendered by long milling times.

### *3.5. Examination of Sinterability and $^{10}B$ Uniformity of Composites*

Figure 8 shows optical micrographs of sintered as well as as-rolled 6061Al/$B_4C$ composite. It can be easily seen that $B_4C$ particles are distributed homogeneously in the alloy matrix and no segregation takes

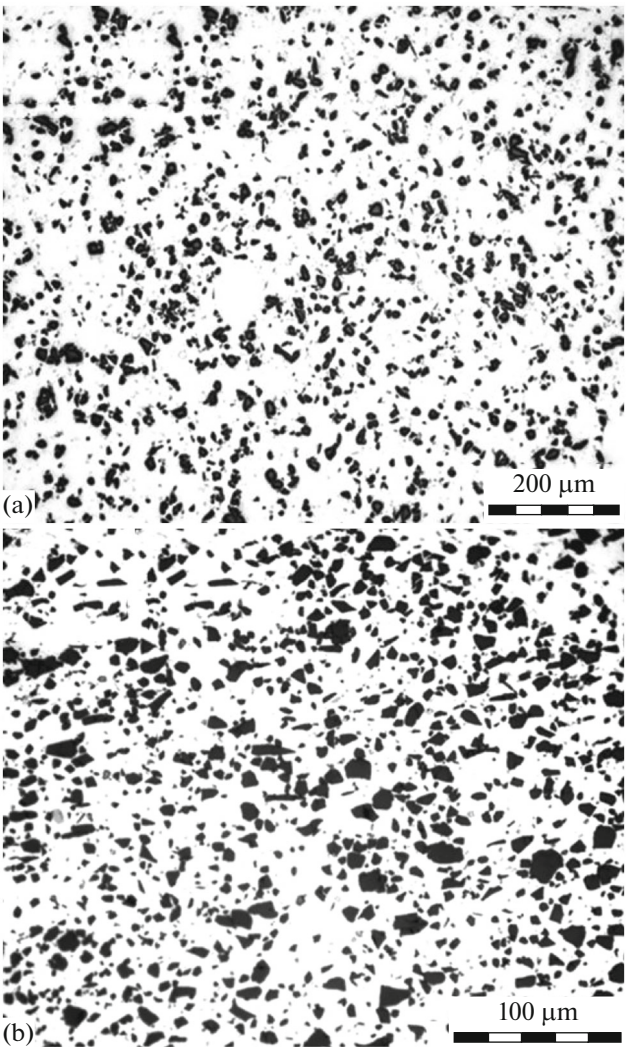


**Fig. 8.** Micrographs of 6061Al/$B_4C$ compact in (a) as-sinter and (b) as-rolled conditions.

place at a particular region. Table 3 shows sintered densities of composites at 585, 610 and 630°C. The density increases with an increase in sintering temperature. This sintering behavior is affected by various factors which are discussed in detail in preceding sections. In composite powders, the local deformation in vicinity of reinforcement particles is enhanced promoting fracture process and diminishing the ductility of composite powder. Moreover, increasing $B_4C$ contents results in more brittle manner and lower powder particle size at same milling conditions. During milling process, the density of dislocations increases due to the presence of hard ceramic particles. The formation of additional dislocations is mainly as a result of difference between coefficient of thermal expansion of matrix and reinforcement [29]. The hard $B_4C$ particles hinder dislocation movements, leading to an increase in dislocation density [30]. Therefore, it is estimated that high reinforcement contents should accelerate sintering process. The sinterability of sintered compacts is evaluated by following equation:

$$\varnothing = \rho_s - \rho_g/\rho_{th} - \rho_g. \quad (15)$$

Where $\rho_s$, $\rho_g$, and $\rho_{th}$ are sintered, green, and theoretical densities, respectively. The results show that sinterability of composite powders decreases with an increase in reinforcement contents (Fig. 9a). This is mainly due to reducing compressibility, as discussed earlier, leading to lower metal-metal contacts. Figure 9b shows that hardness of sintered compacts increases with an increase in hard $B_4C$ contents. Refined microstructure with random interfaces, distribution of fine carbides, and high-density of dislocations results in higher hardness of composites [29, 30].

The effectiveness of neutron absorption of Al 6061–$B_4C$ composites depends on the homogeneity of $B_4C$ particles in composites. The morphology of $B_4C$ particles in composite also plays an important role to neutron absorption. The presence of inhomogeneities and weakness of interface bond between $B_4C$ particles and Al matrix can lead to channeling effect where neutron can pass through boron particles without being absorbed, thus making the composites less effective for neutron shielding. The optical density readings, derived from the neutron radioscopy or radiography are shown in Fig. 10, which verify <10% differences between the minimum and maximum $B_{10}$ areal densities. It implies the uniform distribution of $B_4C$ particles in the developed composite material.

**Table 3.** The densities of Al 6061–*x* wt % $B_4C$ (*x* = 0, 5, 10, 20, 30, 40) composite powders after sintering at different temperatures

| Sample | Green density, g/cm$^3$ | Sintered density, g/cm$^3$ | | |
|---|---|---|---|---|
| | | 585°C | 610°C | 630°C |
| 6061 Al Alloy | 2.58 | 2.59 | 2.62 | 2.64 |
| 6061AA + 05% $B_4C$ | 2.50 | 2.59 | 2.63 | 2.65 |
| 6061AA + 10% $B_4C$ | 2.43 | 2.49 | 2.58 | 2.62 |
| 6061AA + 20% $B_4C$ | 2.31 | 2.35 | 2.52 | 2.55 |
| 6061AA + 30% $B_4C$ | 2.25 | 2.26 | 2.40 | 2.46 |
| 6061AA + 40% $B_4C$ | 2.19 | 2.20 | 2.32 | 2.43 |

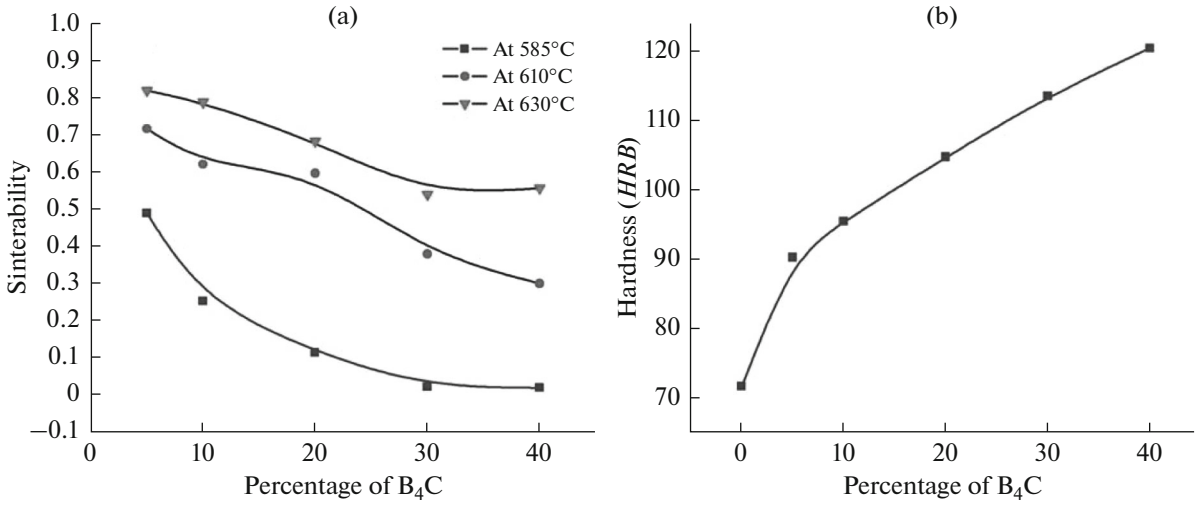


**Fig. 9.** (a) Sinterability curves of Al 6061–$x$ wt % $B_4C$ ($x$ = 0, 5, 10, 20, 30, 40) and (b) hardness of Al 6061–$x$ wt % $B_4C$ ($x$ = 0, 5, 10, 20, 30, 40) sintered at 630°C.

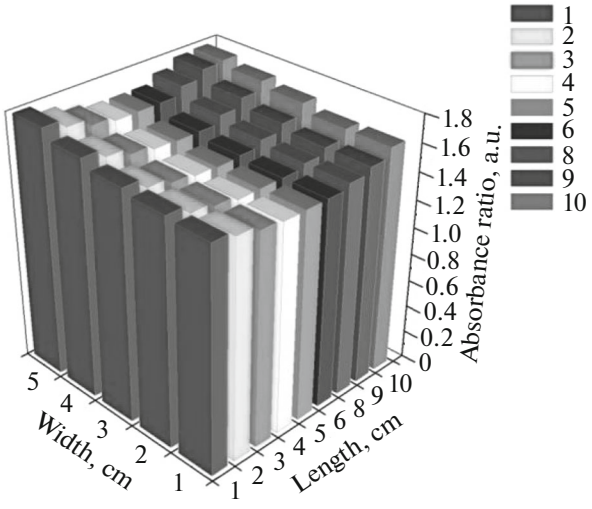


**Fig. 10.** Optical density distribution for 6061Al/$B_4C$ sheet after neutron radiography.

## 4. CONCLUSIONS

The flow characteristics, compressibility, sinterability, and microhardness of AA 6061–$B_4C$ composites, synthesized from mechanically alloyed powders via cold compaction, sintering, and rolling, were investigated in terms of reinforcement additions and milling times. The important conclusions are summarized as follows:

• The agglomerate size of composite powders decreases with $B_4C$ contents added. It is speculated that high hardness and strength of $B_4C$ may penetrate them into alloy matrix resulting in their work hardening and enhancing fracturing mechanism. As hard $B_4C$ particles easily penetrate into soft alloy matrix resulting in decreased volume fraction of free $B_4C$ particles within powder mixture leading to an increased overall particle size distribution.

• The presence of reinforcement particles accelerates the evolution of the apparent density with milling time. The Hausner ratio (HR), estimated to evaluate friction between the particles, decreases with an increase in milling duration and $B_4C$ content due to the changes in morphology and hardness of powders. An increase in $B_4C$ contents results in poor fluidity of composite powders, which is attributed to increased friction among particles arising from irregular powder morphology or larger particle size distributions.

• The incorporation of $B_4C$ considerably reduces matrix particle size resulting in lowering of relative density at low compaction pressures due to work hardening effect. The compressibility behavior of post-compacts as a function of compaction pressure and the $B_4C$ content was analyzed by using several linear and non-linear powder compaction equations. The linear Panelli and Ambrozio Filho, and non-linear Van Der Zwan and Siskens equations give the highest regression coefficients. An increase in $B_4C$ contents decreases the plastic deformation capacity of the matrix at plastic deformation stage due to stress shielding effect of $B_4C$ contents. The rate of plastic deformation coefficient increases with $B_4C$ additions, which is ascribed to morphology changes and refined particle size rendered by long milling times.

• The sinterability of composite powders decreases and hardness of sintered compacts increases with an increase in hard $B_4C$ contents particularly above 10 wt %.

## SUPPORTING INFORMATION:

Figures of particle size distribution of $B_4C$, Morphology of as-received powders, and Micrographs of as-sintered and as-rolled samples. Tables of composition of Al alloy and parameters for neutron radiography.

SUPPLEMENTARY INFORMATION FOR REVIEW

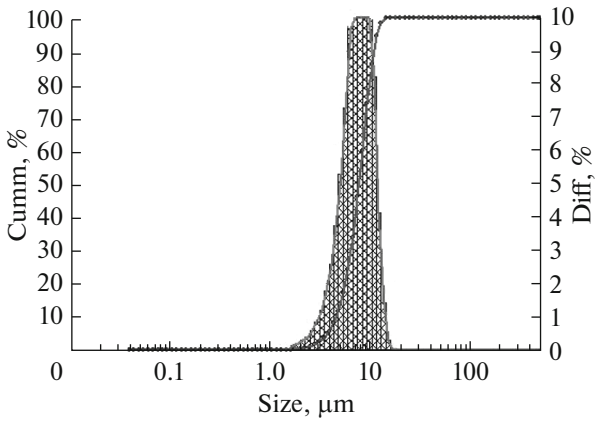


**Fig. S1.** Cumulative and differential particle frequency distribution for boron carbide powder as obtained by laser particle size analysis.

**Table S1.** Composition of 6061Al powder (wt %)

| Alloy | Cu | Mg | Cr | Si | Fe | Zn | Al |
|---|---|---|---|---|---|---|---|
| 6061Al | 0.31 | 1.02 | 0.1 | 0.53 | 0.062 | 0.007 | Balance |

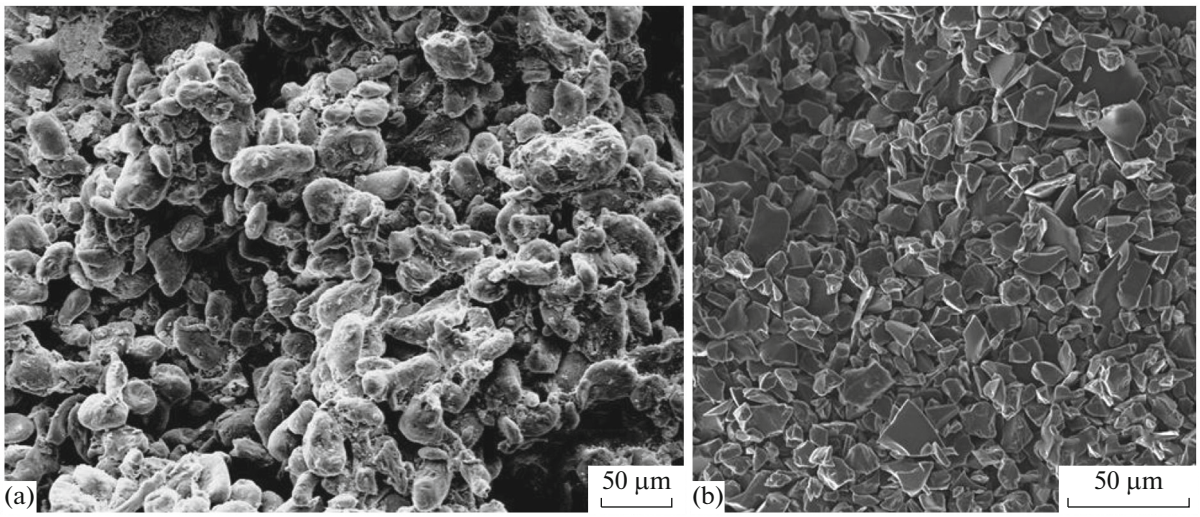


**Fig. S2.** The morphology of as-received powders: (a) 6061Al Alloy and (b) $B_4C$ powders.

**Table S2.** Parameters for Neutron Radiography of 6061Al/$B_4C$ composites

| | |
|---|---|
| Neutron flux | $2 \times 10^6$ n/s cm$^2$ |
| Collimation ratio (L/D) | 10–20 |
| Beam diameter | 20 cm |

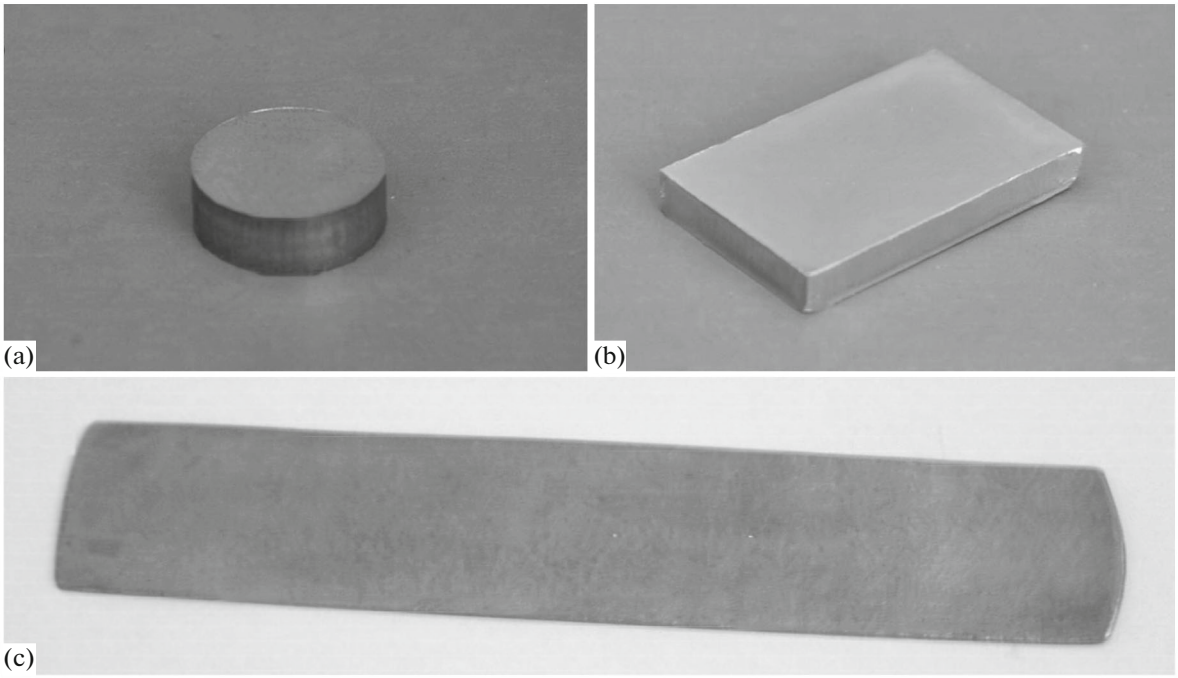


**Fig. S3.** The 6061Al/$B_4C$ composite in (a) as-sintered (19 mm) (b) as-sintered (60 × 40 × 15 mm), (b) as-rolled (20.3 ×58 × 1.65 mm) conditions.

## REFERENCES


1. Miracle, D.B., Metal matrix composites—from science to technological significance, *Compos. Sci. Technol.*, 2005, vol. 65, pp. 2526–2540.
2. Smagorinski, M.E., Tsantrizos, P.G., Grenier, S., Cavasin, A., Brzezinski, T., and Kim, G., The properties and microstructure of Al-based composites reinforced with ceramic particles, *Mater. Sci. Eng. A*, 1988, vol. 244, pp. 86–90.
3. Harrigan, Jr.W.C., Commercial processing of metal matrix composites, *Mater. Sci. Eng. A*, 1988, vol. 244, pp. 75–79.
4. Kaczmar, J.W., Pietrzak, K., and Wlosinski, W., The production and application of metal matrix composite materials, *J. Mater. Process. Technol.*, 2000, vol. 106, pp. 58–67.
5. Chen, X.-G. and Hark, R., Development of Al–30% $B_4C$ metal matrix composites for neutron absorber material, in *Proceedings of Aluminium Alloys: Fabrication, Characerization and Applications*, Yin, W. and Das S.K., Eds., TMS, (2008), pp. 3–7.
6. Bonnet, G., Rohr, V., Chen, X.-G., Bernier, J.L., Chiocca, R., and Issard, H., Use of alcan's Al–$B_4C$ metal matrix composites as neutron absorber material in TN international's transportation and storage casks, *Pack. Trans. Stor. Secur. Radioact. Mater.*, 2009, vol. 20, pp. 98–108.
7. Zhang, J., Guan, R-G., Tie, D., Wang, X., Guan, X., Chen, B., and Chen, Y., Effects of technical parameters of semi-solid stirring and rheo-rolling on microstructure of A356—5 wt % $B_4C$ composite strip, *Mater. Manuf. Proc.*, 2015, vol. 30, pp. 340–345.
8. Lashgari, H.R., Sufizadeh, A.R., and Emamy, M., The effect of strontium on the microstructure and wear properties of A356—10% $B_4C$ cast composites, *Mater. Des.*, 2010, vol. 31, pp. 2187–2195.
9. Toptan, F., Kilicarslan, A., Karaaslan, A., Cigdem, M., and Kerti, I., Processing and microstructural characterization of AA 1070 and AA 6063 matrix $B_4Cp$ reinforced composites, *Mater. Des.*, 2010, vol. 31, pp. S87–S91.
10. Kalaiselvan, K., Murugan, N., and Parameswaran, S., Production and characterization of AA 6061–$B_4C$ stir cast composite, *Mater. Des.*, 2011, vol. 32, pp. 4004–4009.
11. Khakbiz, M. and Akhlaghi, F., Synthesis and structural characterization of Al–$B_4C$ nano-composite powders by mechanical alloying, *J. Alloys Compd.*, 2009, vol. 479, pp. 334–341.
12. Mohanty, R.M., Balasubramaniana, K., and Seshadri, S.K., Boron carbide-reinforced aluminium 1100 matrix composites: Fabrication and properties, *Mater. Sci. Eng. A*, 2008, vol. 498, pp. 42–52.
13. Jeyasimman, D., Sivasankaran, S., Sivaprasad, K., Narayanasamy, R., and Kambali, R.S., An investigation of the synthesis, consolidation and mechanical behaviour of Al 6061 nanocomposites reinforced by TiC via mechanical alloying, *Mater. Des.*, 2014, vol. 57, pp. 394–404.
14. Sivasankaran, S., Sivaprasad, K., Narayanasamy, R., and Iyer, V.K., Evaluation of compaction equations and prediction using adaptive neuro-fuzzy inference system on compressibility behavior of AA 6061100–*x*–*x* wt % $TiO_2$ nanocomposites prepared by mechanical alloying, *Powder Technol.*, 2011, vol. 209, pp. 124–137.

15. Zhang, Z., Fortin, K., Charette, A., and Chen, X.-G., Effect of titanium on microstructure and fluidity of Al–$B_4C$ composites, *J. Mater. Sci.*, 2011, vol. 46, pp. 3176–3185.

16. Varol, T. and Canakci, A., Effect of particle size and ratio of $B_4C$ reinforcement on properties and morphology of nanocrystalline Al2024–$B_4C$ composite powders, *Powder Technol.*, 2013, vol. 246, pp. 462–472.

17. Asghar, Z. and Zahid, G.H., Rafi-ud-din, Ahmad, E., and Mehmood, M., Effect of degassing parameters on the sinterability of Al/$B_4C$ composite, *Powder Metall.*, 2015, vol. 58, pp. 36–40.

18. Sivasankaran, S., Sivaprasad, K., Narayanasamy, R., and Iyer, V.K., An investigation on flowability and compressibility of AA6061 100–*x*–*x* wt % $TiO_2$ micro and nanocomposite powder prepared by blending and mechanical alloying, *Powder Technol.*, 2010, vol. 201, pp. 70–82.

19. Chen, H.S., Wang, W.X., Li, Y.L., Zhang, P., Nie, H.H., and Wu, Q.C., The design, microstructure and tensile properties of $B_4C$ particulate reinforced 6061Al neutron absorber composites, *J. Alloys Compd.*, 2015, vol. 632, pp. 23–29.

20. Gan, K. and Gu, M., The compressibility of Cu/SiCp powder prepared by high-energy ball milling, *J. Mater. Process. Sci. Technol.*, pp. 199, 173.

21. Zhao, N., Nash, P., and Yang, X., The effect of mechanical alloying on SiC distribution and the properties of 6061 aluminum composite, *J. Mater. Process. Sci. Technol.*, 2005, vol. 170, pp. 586–592.

22. Abenojar, J., Velasco, F., and Mart'inez, M.A., Optimization of processing parameters for the Al + 10% $B_4C$ system obtained by mechanical alloying, *J. Mater. Process. Sci. Technol.*, 2007, vol. 184, pp. 441–446.

23. Alizadeh, A. and Taheri-Nassaj, E., H. Baharvandi, R., Preparation and investigation of Al–4 wt % $B_4C$ nanocomposite powders using mechanical milling, *Bull. Mater. Sci.*, 2011, vol. 34, pp. 1039–1048.

24. Moazami-Goudarzi, M. and Akhlaghi, F., Effect of nanosized SiC particles addition to CP Al and Al–Mg powders on their compaction behavior, *Powder Technol.*, 2013, vol. 245, pp. 126–133.

25. Joa, B., Fogagnolo, B., Ruiz-Navas, E.M., Robert, M., Jose, H., and Torralba, M., The effects of mechanical alloying on the compressibility of aluminium matrix composite powder, *Mater. Sci. Eng. A*, 2003, vol. 355, pp. 50–55.

26. Fogagnolo, J.B., Velasco, F., Robert, M.H., and Torralba, J.M., Effect of mechanical alloying on the morphology, microstructure and properties of aluminium matrix composite powder, *Mater. Sci. Eng. A*, 2003, vol. 342, pp. 131–143.

27. *Powder metal technologies and applications, ASM Handbook*, vol. 7. Materials Park (OH), 1998.

28. Kawakita, K. and Ludde, K.-H., Some considerations on powder compression equations, *Powder Technol.*, 1971, vol. 4, pp. 61–68.

29. Elomari, S., Skibo, M.D., Sundarrajan, A., and Richards, H., Thermal expansion behavior of particulate metal-matrix composites, *Compos. Sci. Technol.*, 1998, vol. 58, pp. 369–376.

30. Hong, S.J. and Kao, P.W., SiC-reinforced aluminum composite made by resistance sintering of mechanically alloyed powders, *Mater. Sci. Eng. A*, 1989, vol. 119, pp. 153–159.